Street canyon ventilation: Combined effect of crosssection geometry and wall heating

ORIGINAL ARTICLE

Street canyon ventilation: combined effect of cross-section geometry and wall heating

Sofia Fellini[1,2] | Luca Ridolfi[2] | Pietro Salizzoni[1]

[1]Laboratoire de Mécanique des Fluides et d'Acoustique, UMR CNRS 5509, Université de Lyon, Ecole Centrale de Lyon, INSA Lyon, Université Claude Bernard Lyon I, Ecully, France

[2]Department of Environmental, Land, and Infrastructure Engineering, Politecnico di Torino, Turin, Italy

Correspondence
Sofia Fellini,Department of Environmental, Land, and Infrastructure Engineering, Politecnico di Torino, Turin, Italy
Email: sofia.fellini@polito.it

Funding information

Understanding the dynamics of mass exchange between a street canyon and the overlying atmosphere is crucial to predict air quality in urban areas. Despite the large number of studies on this topic, there are many aspects that still need to be clarified. Among these, one is certainly the role of thermal stratification in street canyon ventilation. In order to fill this gap, this study evaluates how the combined effect of street canyon geometry, wall roughness and differential heating of the building façades influences pollutant dispersion within the canyon and out of it. The study was carried out in a wind tunnel, adopting an idealized urban geometry made-up of square bars placed normal to the wind direction. The boundary conditions inside the canyon were modified by heating its windward and leeward walls, by changing its aspect ratio and by introducing roughness elements at walls. A passive scalar was injected from a line source at ground level. The flow and concentration fields were measured in a cross-section of the canyon. Characteristic exchange velocities within the canyon and towards the external flow were estimated comparing the experimental data with an analytical model for the cavity wash-out. Results show that the transition from one recirculating cell to two counter-rotating cells inhibits canyon ventilation, with a consequent increase in pollutant concentration at the pedestrian level. This transition occurs as the

cavity aspect ratio increases and is facilitated by adding roughness elements at the windward wall. Heating the leeward wall has negligible effects on canyon ventilation. Heating the windward wall accelerates pollutant removals in square cavities, while it contributes to a worsening of air quality in narrow cavities. Finally, the wash-out times of the cavity are discussed in terms of a relative contribution of the mean advective motion and its turbulent counterpart.

KEYWORDS
Street canyon, Urban air pollution, Turbulent transfer of passive scalars, Wind-tunnel experiments, Thermal effects, Solar radiation

1 | INTRODUCTION

In 2050, more than 70% of the world population will live in urban areas [23]. Despite recent efforts in environmental policies, air pollution in cities still represents the biggest environmental risk to health [78]. In particular, citizens in developing countries are the most impacted by poor air quality.

To address this rapid urbanization, solutions for more sustainable cities are extensively sought [e.g., 21, 10, 9]. The assessment and implementation of these mitigation strategies require a deep understanding of the urban microclimate [65, 57, 22] which is the result of the complex interaction between physical phenomena (e.g., wind, atmospheric stability, solar radiation) and the city (e.g., buildings, anthropogenic emissions, urban vegetation).

In this framework, the prediction of pollutant transfer within and above a street canyon is crucial to develop urban dispersion models for operational purposes [80, 74, 75, 72, 18]. The street canyon is the fundamental unit of the urban geometry. It is composed by a narrow street flanked by buildings on both sides, creating a canyon-like environment. In street canyons, the concentration of pollutants is high due to the presence of (ground level) vehicular and anthropogenic emissions and to the weak air ventilation caused by a recirculating motion between the buildings. The close proximity between emitters (vehicles, chimneys) and receptors makes these regions extremely vulnerable to health risks [24]. Generally, the maximum concentration occurs when the wind blows perpendicular to the street canyon, inducing a recirculating flow that confines the transport of pollutants. Another critical case is represented by very long streets, in which pollutant accumulation, due to the longitudinal wind, is responsible for concentrations close to or even higher than those observed with a wind direction perpendicular to the street axis [73].

While horizontal advection at the lateral ends of a street canyon is the dominant ventilation mechanism for longitudinal and oblique wind directions [e.g., 12], when the wind is perpendicular to the street, the air quality mainly depends on the vertical pollutant exchange with the atmosphere above roof-level. Several studies focused on the influence of different dynamical and geometrical parameters on this vertical transfer. Considering the problem as two-dimensional, the flow dynamics are analysed in a generic cross-section of

the canyon, i.e. in a two-dimensional cavity. The effect of the cavity geometry on the flow dynamics within the canyon has become a classical case-study in fluid mechanics. A number of works [27, 56, 30, 4] has demonstrated that the formation of secondary vortices in narrow cavities inhibits the canyon ventilation. The studies of Murena and Mele [49] and Llaguno-Munitxa et al. [42] evidenced the role of roughness elements (e.g., balconies) on the building walls in reducing the pollutant transfer from the street to the above atmosphere. In addition to the influence of large and small geometrical scales, the efficiency of street canyon ventilation has been investigated with respect to several other aspects. Among these, we cite here the experiments of Salizzoni et al. [63, 62], who investigated the role of the external turbulence, Solazzo et al. [70], who performed numerical simulations about the effect of traffic induced turbulence on dispersion processes within the street, and Gromke and Ruck [20], who tried to clarify the impact of trees on the canyon ventilation.

Besides the analysis of these dynamical mechanisms, a growing interest has been devoted to the study of buoyancy effects on the air flow within the canyon. Thermal fluxes generate buoyancy forces that have a relevant influence especially in low wind condition. These effects are primarily associated to solar radiation which induces temperature differences between the canyon walls of about 15 K at mid latitudes [43, 55]. A deep understanding of the interaction between wind and buoyancy forces within the streets is crucial for the implementation of natural or hybrid ventilation techniques [26, 19], for the improvement of energy performance in buildings [65], and for mitigating the heat island effect through in-canyon vegetation [2, 36] and urban planning [76].

Variations in the flow streamlines within a street canyon due to heat fluxes at the canyon walls and bottom were investigated numerically by the RANS models of Sini et al. [67] and Kim and Baik [32]. Sini et al. [67] found that when a wind is blowing perpendicular to the canyon and the downstream wall is heated, two counter-rotating vortices are formed. The CFD simulations of Xie et al. [79] confirmed these findings but observed that these secondary structures were overestimated with respect to the wind-tunnel observations of Kovar-Panskus et al. [33]. Solazzo and Britter [69] simulated weak buoyancy effects in the canyon to estimate a typical vertical exchange velocity. More recently, the LES studies of Cai [11] and Li et al. [39, 38] provided insights into the turbulence structure within a heated canyon, while Nazarian et al. [51] investigated the effect of three dimensional surface heating. With numerical simulations, a great variety of scenarios can be analysed. However, these simulations are very sensitive to the domain size [16], to the sub-grid model and to the treatment of the boundary conditions.

Field studies on the effect of thermal fluxes in street canyons were conducted in different European and Asian cities [50, 43, 55, 52]. In these studies, the influence of thermal fluxes seemed to be limited to a thin layer close to the heated wall, and the occurrence of secondary recirculating structures was not detected.

Few wind-tunnel experiments were performed to investigate the role of wall heating on the flow structure within a street canyon. This is mainly due to practical difficulties in complying with the similarity criteria for the internal Froude number, i.e. the dimensionless number expressing the ratio of inertial to buoyancy forces (see Section 2.3). In fact, very large temperature differences within the canyon are required to reproduce realistic buoyancy conditions in wind tunnel models with high scaled street canyons. Uehara et al. [77] analysed the effects of atmospheric stability on the the flow within a street canyon heating the floor of the wind tunnel. Kovar-Panskus et al. [33] proposed a wind-tunnel experiment with the direction of the wind normal to the canyon and a differential heating of the cavity walls. In the experiment, the downstream wall of a square canyon was heated and four external velocities were applied in order to generate different buoyancy conditions. They observed the formation of a stagnant flow at the bottom of the cavity, as the Froude number decreases. By means of PIV (Particle Image Velocimetry) measurements, Allegrini et al. [3] investigated the flow field in

a square cavity for a wider range of configurations: heating of the (i) upstream wall, (ii) downstream wall, (iii) canyon ground, and (iv) all three surfaces together. The formation of a second counter-rotating vortex was evident for the configuration with the heating of the windward wall. In all cases, an increase in the turbulent kinetic energy inside the cavity was measured. Similar results for the flow field were found by Marucci and Carpentieri [44], who in addition analysed the effect of stratification in the approaching flow. By the release of a tracer from a ground level source, dispersion measurements were also performed.

Besides these recent works, the shortage of laboratory experiments represents a significant limitation for the validation of the widespread numerical studies. To date, we observe the lack of a comprehensive analysis of the combined effect of the street canyon geometry and the buoyancy conditions within it. These factors proved to be key in determining the fluid dynamical conditions in the street canyon.

In this picture, the goal of this study is to evaluate, by means of wind-tunnel experiments, how different geometry and heat conditions within a two-dimensional street canyon determine the flow and the dispersion of a passive scalar within the cavity itself. To this aim, the flow field for an airflow perpendicular to the canyon is analysed for eight different aspect ratios of the cavity in isothermal conditions. The effect of roughness elements on the canyon walls is also investigated for these configurations. For a square and a narrow cavity, thermal effects are examined. The upwind and downwind walls are alternatively heated and different thermal fluxes are experimented. The spatial coherence of the turbulent field is investigated by means of PIV. Steady and unsteady measurements of concentration are performed in the cavity with a Flame Ionisation Detector (FID) system, in order to investigate both the spatial distribution and the temporal evolution of pollutants released at the ground level.

The variety of experimental configurations, the different measured quantities and their analysis sheds light on the fluid-dynamical mechanisms that govern the wash-out of a two-dimensional street canyon for a perpendicular wind direction. This is done to improve the modelling of air pollution and heat transfer in cities.

2 | METHODOLOGY

2.1 | Experimental setup

The experiments were performed in a closed-circuit wind tunnel (Figure 1) at the laboratory LMFA (Laboratoire de Mécanique des Fluides et d'Acoustique) at the École Centrale de Lyon. The test section of this tunnel is 8 m long, 1 m high and 0.7 m wide. Irwin spires [29] with a height of 0.4 m were placed at the entrance of the test section. A total of 65 aluminium bars were arranged normal to the wind direction, along the entire length of the wooden floor of the wind tunnel. The bars were of section 0.06 m x 0.06 m, with a length (L) of 0.7 m extending over the entire width of the tunnel, and with a spacing of 0.06 m between them. In this way, we obtained a regular set of parallel street canyons with a constant aspect ratio of one, with the exception of the canyon where the measurements were taken which had a variable aspect ratio. This canyon was located 5 m downstream of the vortex generators, i.e. downwind of an urban canopy of about 40 canyons. In this way, the fully development of the approaching flow was guaranteed [46, 59] and a neutral atmospheric boundary layer with depth $\delta = 0.6$ m was obtained. The blockage ratio of the model to the cross-section of the wind tunnel was 6%. Before starting the experiments, we ensured that the incident velocity field was two-dimensional by measuring velocity profiles upstream and downstream of the canyon at different transversal positions. These velocity profiles confirmed that the flow field was uniform in the transverse direction, with variations of less

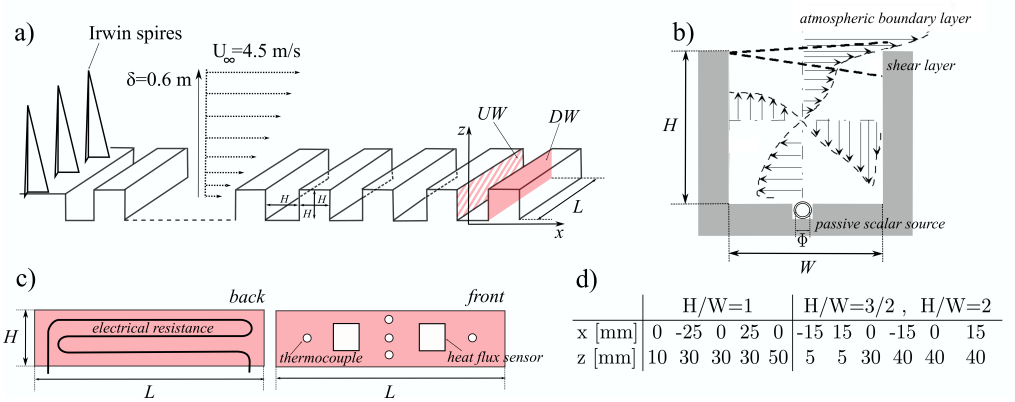

FIGURE 1 a) Overview of the wind tunnel installation with the position of the street canyon. b) Sketch of the canyon cross-section with the qualitative representation of the two-dimensional flow. The line source is located in a slot cut in the tunnel floor. c) Sketch of the set-up for the configurations with heating of the downwind wall (DW). d) Horizontal (X) and vertical (Z) coordinates of the points where the wash-out curves were measured.

than 1% for the mean flow and 5% for the turbulence quantities. Moreover, concentration measurements were performed along the longitudinal axis of the canyon at various heights (with the linear source of tracer placed at ground level) demonstrating the two-dimensional nature of the mean concentration field within the canyon.

The height (H) of the canyon in which the measurements were performed was 0.06 m (i.e. one tenth of the boundary layer height), while its width (W) varied between 0.03 m and 0.06 m.

The lower part of the vertical profile of the mean horizontal velocity that develops above the transversal bars can be modelled by the classic logarithmic profile: $U(z) = (u_*/\kappa)\ln[(z-d)/z_0]$, where z_0 is the roughness length, u_* is the friction velocity, d is the displacement height and κ is the Von Kármán constant. The incoming wind profile was kept constant in this study. The free stream velocity at the top of the boundary layer (U_∞) was kept fixed and equal to 4.5 m/s. The friction velocity $u_* = 0.22$ m/s was determined from the Reynolds stress profile, while $z_0 = 0.1$ mm and $d = 57$ mm were evaluated by fitting the logarithmic profile to the experimental data in the lower part of the boundary layer flow. Note that the incoming flow corresponds to that of Configuration 1 in [64], to which the reader is addressed for further details on the statistics of the velocity field.

A pollutant release was simulated by the injection of ethane from a linear ground level source placed at the centre of the canyon. The linear source was a porous polymeric tube with diameter $\Phi = 4$ mm, located in a slot cut in the tunnel floor so as not to alter the velocity field (see Figure 1.b). The tracer gas supply was monitored continuously using a Brooks flow meter, and the experiments were performed with a mass flux of 2.8 mg/s, giving a mass flow rate per unit of length $\dot{M}_q = 4$ mg/s·m. The fluctuations in the mass flow rate were less than 1%.

To investigate buoyancy effects inside the canyon, each lateral wall of the street canyon was heated at a time. A heating mat was attached at the back of the heated wall, inside the lateral aluminium bar (as shown in Figure 1.c). Constant and controlled heat fluxes from the thermal resistance were produced exploiting Joule heating.

Experiments with roughness elements to the side walls were performed to analyse the effect of small scale

geometry on the cavity flow. In these experiments, a corrugated cardboard sheet was fixed to one or the other lateral wall of the canyon.

2.2 | Measurement techniques

The velocity field within the cavity and in the lowest part of the boundary layer was measured using a Particle Image Velocimetry (PIV) system. Two coupled YAG laser sources provided pairs of laser pulses at a frequency of 4 Hz. The visualization light sheet was perpendicular to the canyon axis and measured 1 mm in width. The flow was seeded with micron-sized droplets produced by a smog generator. The observation field measured approximately 0.12 m x 0.12 m (2H x 2H), and was filmed at a resolution of 1280 x 1024 pixels. Due to the reflection of the laser light on the cavity surfaces, velocity measurements very close to the walls had to be discarded. However, the disturbed area consisted of a thin layer of one to two millimetres near the walls, thus not compromising the analysis of the velocity field as a whole. The images were processed using cross-correlation. The interrogation window was fixed at 16 x 16 pixels, corresponding to an averaging area of 0.9 mm x 0.9 mm. The interrogation areas overlapped by 50% so that in total, each velocity field computation yielded a set of 240 x 240 vectors. The velocity field was recorded with 1000 double frame images at a frequency of 4 Hz, i.e. two images were captured each 0.25 seconds, with a time interval of 30 μs between the two shots. From these 1000 instantaneous velocity fields, we computed for each (x, z) point reliable flow statistics up to the third order moment of the velocity field, as shown in Figure S1 in the Supporting Information (SI). In this way, we obtained the horizontal (U) and vertical components (V) of the mean velocity, their variances σ_u^2 and σ_v^2, and the mean vorticity field $\overline{\omega} = (\partial \mathrm{V}/\partial x - \partial \mathrm{U}/\partial z)\mathbf{k}$. The turbulent kinetic energy field (TKE) was computed as TKE$= 0.5(\sigma_u^2 + \sigma_v^2)$. In this expression, the velocity variance in the third direction (σ_w^2) is missing as the velocity field is measured only in the plane perpendicular to the canyon axis. While providing information on the spatial structure of the flow (e.g., the vorticity field), PIV system suffers some limitations when used to elaborate the turbulence statistics, since a lower number of samples per location is available compared to other measurement systems, as Hot Wire Anemometry (HWA) or Laser Doppler Anemometry (LDA) [28]. Best practices were adopted to minimize the errors in the measurements [1, 60]. Moreover, we tested the performances of the PIV system by comparing the vertical profile of TKE with measurements from an Hot Wire Anemometer system [53]. Starting from these measurements, we estimated a percentage error almost everywhere below 5% (with peaks of 10%) for the TKE.

Concentration within the cavity was measured using a Flame Ionisation Detector (FID) system [17]. FID is commonly used for concentration measurements in urban-like geometries [e.g., 59, 12]. A FID system with a sampling frequency of about 800 Hz [54] was used in this study, thus allowing the reconstruction of a 400 Hz concentration signal ($\simeq$ 1 ms time response of the instrument). Ethane was chosen as a passive tracer, since its molecular weight is nearly the same of air. To avoid the disruption of the local flow, a straight 30 cm long sampling capillary tube was mounted on the FID head, which was positioned above the test section so as not to affect the flow field. Steady and unsteady experiments were carried out. In steady conditions, the injection of ethane from the ground level source was kept constant and the mean concentration within the cavity was measured on a regularly spaced grid (1 cm x 1 cm). In each sampling point, a FID acquisition time of 60 seconds was sufficient to provide averaged statistics. The mean concentration field was then obtained by spatial interpolation between the sampling points. The experiments in unsteady conditions were performed to estimate the typical wash-out velocity of the cavity. As in [61] and [63], we measured the temporal evolution of ethane concentration at different positions within the cavity as it emptied. In Figure 1.d, the position of the sampling

points is reported. The experiment was performed as follows: (i) ethane was first injected into the canyon until the concentration field reached a stationary state; (ii) the injection of ethane was then interrupted by means of a valve; (iii) the temporal evolution of the concentration was recorded by the FID probe for a time interval of 15 seconds, in a single sampling point. For each sampling point, passages (i) to (iii) were repeated between 30 and 50 times to allow an ensemble average for the signal. By the subtraction of the background concentration (C_b) and the normalization to the initial value, i.e. the initial concentration in stationary conditions (C_{ss}) in the sampling point, the dimensionless (ensemble-averaged) wash-out curve was finally obtained.

For the experiments with heating of the side walls, two heat flux sensors of size of 3 cm x 3 cm, thickness 0.3 mm, and sensitivity $5\text{x}10^{-3}\ V/(W/m^2)$ were placed on the heated wall, on the side facing the canyon (as shown Figure 1.c). These sensors monitored the constant thermal flux at the heated wall. More details about the heat fluxes measured during the experiments are reported in the SI. For temperature measurements, 5 T-type thermocouples were placed on the heated wall (the position of the sensors is shown in Figure 1.c) and a single thermocouple on the non-heated wall. Moreover, each heat flow sensor was also equipped with a thermocouple. Temperature was measured for the entire duration of the experiment and remained on average constant over time ($\simeq \pm 1$ K). A maximum spatial difference of temperature of around ± 2 K degrees was observed along the longitudinal coordinate of the wall. Negligible effects in the immediate vicinity of the walls were observed in the flow field due to the installation of the thermocouples and the heat flux sensors.

2.3 | Experimental conditions

Street canyon ventilation is expected to depend on the variables that characterize the turbulent flow within the street canyon. These are: the height (H) and the width (W) of the canyon cross-section, the kinematic viscosity (ν) and the thermal (α) and mass (D) diffusivity of the fluid, a characteristic velocity scale ($\mathcal{U}$), the roughness height (h_r) of the canyon walls, the gravitational acceleration (g), the reference air temperature (T_0), and the surface temperature of the possible heated wall (T_W). Introducing the velocity u_d as the rate of vertical bulk exchange of pollutants between the street canyon and the overlying atmosphere, we can therefore seek to define the following dependence:

$$u_d = f(H, W, \nu, \alpha, D, \mathcal{U}, h_r, g, T_0, T_W), \tag{1}$$

which, according to the Buckingham Π theorem, can be expressed in the following non-dimensional form:

$$\frac{u_d}{\mathcal{U}} = f\left(\frac{H}{W}, \frac{h_r}{H}, Pr = \frac{\nu}{\alpha}, Sc = \frac{\nu}{D}, Re = \frac{\mathcal{U}H}{\nu}, Fr_i = \frac{\mathcal{U}}{\sqrt{gH\frac{\Delta T}{T_0}}}\right), \tag{2}$$

with $\Delta T = T_W - T_0$. The physics of the phenomenon depends on two geometrical parameters, and four dynamical parameters. The geometrical parameters are the aspect ratio (H/W) of the canyon cross-section and a characteristic roughness (h_r/H) of the canyon walls. These parameters account for the effect of large and small geometrical scales, respectively. The three dynamical parameters are the Prandtl (Pr), Schmidt (Sc), Reynolds (Re) and internal Froude (Fr_i) numbers. The definition of the velocity scale $\mathcal{U}$ in the Reynolds and Froude numbers is not trivial for a flow within a cavity. Kovar-Panskus et al. [33] and Allegrini et al. [3] assumed $\mathcal{U}$ as the velocity at the top of the external boundary layer flow (U_∞). However, this is not necessarily a characteristic scale for the flow in the canyon since the same U_∞ could produce different boundary layer flows,

and therefore different canyon flows, depending on the roughness of the obstacles upwind the canyon. Other authors [13, 68] considered as velocity scale the wind speed at the building height (U_H). Salizzoni et al. [62] observed that there is not a unique velocity scale that correctly characterizes the turbulent flow within the canyon. They also found that the turbulent kinetic energy (TKE) within the cavity scales well on the friction velocity u_*. Since the wash-out process is expected to depend on the TKE [63], we take, in this study, the friction velocity u_* as velocity scale.

The Prandtl and Schmidt numbers (see Equation 2) are almost constant within the range of temperature we consider in our experiments ($Pr \simeq 0.7$ and $Sc \simeq 0.9$). The Reynolds number undergoes slight variations due to small differences in the velocity profile realized in the wind-tunnel and to the increase of ν with temperature. In wall-heated configurations, sharp temperature gradients are measured in close proximity to the heated wall (within 0.5 cm from the wall), while the average temperature in the cavity increases by a maximum of 50 K with respect to the temperature outside the canyon. Taking into account the increase in ν with this temperature variation, we obtain Reynolds numbers based on the wind speed at the building height ($Re_H = U_H H/\nu$) in the range 5700-7200. Castro and Robins [13] and Marucci and Carpentieri [44] showed that, for Re_H larger than 4000, no Reynolds number effects were discernible for the flow field within a cavity of unit aspect ratio. Considering a Reynolds number based on the free stream velocity ($Re_\infty = U_\infty H/\nu$), Allegrini et al. [3] obtained a Reynolds independent flow, in a square cavity, for Re_∞ above 13000. In our setup, Re_∞ is in the range 14200-18000. The narrow street canyon is expected to be more vulnerable to the Re independency. However, Barlow and Belcher [7] found a Re independent transfer velocity in a canyon with $H/W = 2$ for Re_H lower than those of this experiment. After these considerations, we can therefore assume that the flow is Reynolds independent in our experiment.

The experiments were performed for aspect ratios varying between 1 and 2. These are the typical geometries in European urban environments [73]. The effect of roughness on the canyon walls was tested by adding small scale roughness elements on one or the other sidewall. Experiments with two different roughness scales (h_r) were performed: corrugated cardboard sheets with flute thickness of 2 mm ($h_r/H = 1/30$) and 5 mm ($h_r/H = 1/12$) were used to simulate an idealised façade roughness. Notice that a roughness scale of 5 mm on the 60 mm high canyon wall is representative of a characteristic balcony depth of 1.5 m in a street canyon with 20 m high side buildings [e.g. 49]. Three heating configurations were investigated: (i) the isothermal case, (ii) the heating of the upwind (UW) wall, and (iii) the heating of the downwind (DW) wall. In the last two cases, different thermal fluxes were imposed at the heated wall. The resulting temperature differences ($\Delta T = T - T_0$) are reported in Table 1, with the corresponding Fr_i. The reference temperature T_0 ($T_0 \simeq 300$ K) varied from day to day, and was measured away from the street canyon.

It is worth noting that, since the velocity scale is different, the values of Fr_i considered here cannot be directly compared to those of Kovar-Panskus et al. [33], Allegrini et al. [3], and Marucci and Carpentieri [44]. However, taking U_∞ as velocity scale in order to compare the conditions of the different experiments, we obtain Fr_i values of an order of magnitude higher than those obtained in the above mentioned works, since the size of the canyon in our experiments is considerably smaller. Taking the Froude number as similarity criterion, our experimental conditions correspond to temperature differences from 4 to 15 Kelvin degrees in realistic street canyons flanked by 20-meter high buildings, and subject to a wind profile characterized by $u_* = 1$ m/s. These temperature differences are typically reached near sun-heated walls in Mediterranean cities [43, 55].

$\frac{H}{W}$	No Roughness						Roughness	
	No Heating	DW Heating (ΔT) [K]			UW Heating (ΔT) [K]		UW	DW
		70	140	170	240	140	240	
1	✓	$Fr_i = 0.62$	X	$Fr_i = 0.40$	$Fr_i = 0.34$	$Fr_i = 0.44$	$Fr_i = 0.34$	✓	✓
1.5	✓	$Fr_i = 0.57$	$Fr_i = 0.40$	$Fr_i = 0.37$	$Fr_i = 0.31$	$Fr_i = 0.45$	$Fr_i = 0.34$	✓	✓
1.3, 1.4, 1.6, 1.7, 1.8, 2	✓	X				X		✓	✓

TABLE 1 Experimental configurations. The check mark indicates the investigated experiments, while the X marks those not considered. The internal Froude number is specified for the configurations with differential heating of the walls. UW and DW stand for Upwind and Downwind wall, respectively.

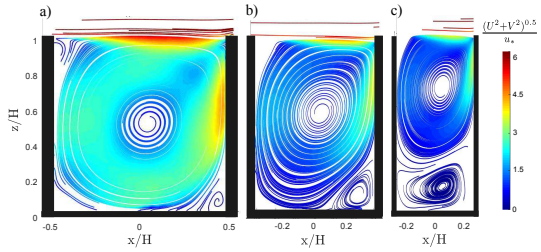

FIGURE 2 Streamlines of the mean velocity field for the aspect ratios (a) H/W=1, (b) H/W=1.5 and (c) H/W=2.

3 | EFFECT OF LARGE AND SMALL GEOMETRICAL SCALE

3.1 | Effect of the large geometrical scale

As well documented by previous experimental and numerical studies [45, 27, 56, 67], the topology of the mean velocity streamlines within the cavity varies with the canyon geometry. In our experiments, the mean flow shows that, for an aspect ratio H/W equal to 1, most of the cavity is filled by a large rotating cell, with its centre close to the cavity centre (Figure 2.a). As the street aspect ratio increases, a second counter-rotating cell appears at the bottom of the cavity (Figure 2.b-c). The velocities in this second vortex are much lower than those in the upper vortex. In our experiments, the transition from one main circulating cell to two counter-rotating cells emerges for an aspect ratio H/W greater than 1.8. For this aspect ratio, the sign of the vertical velocity profile in $x = 0$ (Figure 3) changes three times, revealing that the second cell is fully established in the centre of the lower part of the canyon. A similar value (i.e. $H/W = 1.7$) was found numerically by Sini et al. [67], while Lee and Park [35] found that this transition takes place for $H/W \simeq 2.1$. As will be discussed below, this transition depends on the amount of clockwise vorticity entering the canyon, i.e. on the approaching flow as well as on the cavity aspect ratio. This explains why discrepancies on the H/W value for transition occur in the different studies.

In all the considered geometries, the turbulent kinetic energy within the cavity (Figure 4) is up to an order of magnitude lower than in the external flow (i.e. for $z/H > 1$). This finding is in accordance with the experimental results obtained by Salizzoni et al. [62], Allegrini et al. [3] and Marucci and Carpentieri [44]. In the here analysed configurations, the transversal bars are very close, so that the flow regime in the street canyon is a skimming flow [56]. In skimming flow, the size of the turbulent eddies that develop in the shear layer at the top of the cavity is limited to the horizontal spacing between the obstacles. Therefore, the eddies

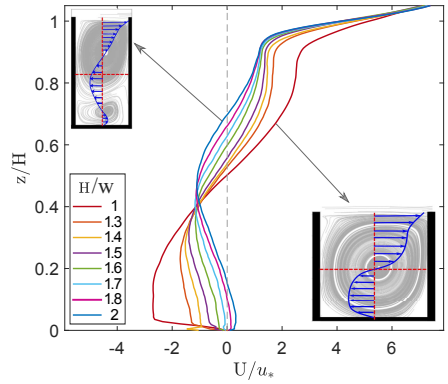

FIGURE 3 Vertical profile of the mean horizontal velocity at $x = 0$ for different aspect ratios.

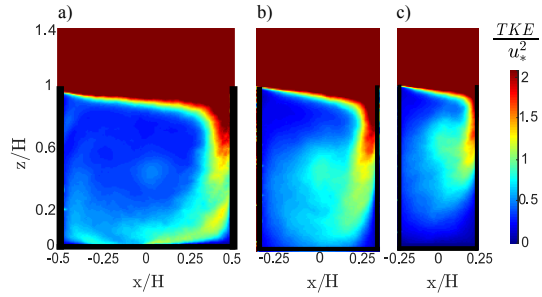

FIGURE 4 Turbulent kinetic energy for the aspect ratios (a) H/W=1, (b) H/W=1.5 and (c) H/W=2.

in the shear layer are not sufficiently developed to couple with the turbulent eddies in the external flow [e.g., 37, 62]. As a consequence, the shear layer shelter the flow within the cavity and the fluctuating flow within the canyon is isolated from the external flow. The main interaction between the cavity flow and the external flow is confined to the upper edge of the downwind wall. Here, a TKE plume spreads down into the cavity all along the canyon wall. For a square cavity, the plume reaches the downwind lower corner and it affects the entire cavity at the street level (panel a in Figure 4). With increasing aspect ratios, the formation of the second counter-rotating cell inhibits the turbulence transfer in the lower part of the canyon (panel c).

The formation of the second cell can be conveniently described in terms of vorticity more readily than in terms of velocity. The vorticity transport equation for a zero-divergence flow is

$$\frac{D\boldsymbol{\omega}}{Dt} = \boldsymbol{\omega} \cdot \nabla \mathrm{u} + \nu \nabla^2 \boldsymbol{\omega} - \mathrm{S_T} \times \mathrm{g}, \tag{3}$$

where $\boldsymbol{\omega}$ is the vorticity, g is the gravity vector, and $\mathrm{S_T}$ is a function of the temperature gradient: $\mathrm{S_T} = \nabla T / T$. The rate of change of vorticity (on the left-hand side of Equation 3) is therefore given by the stretching of

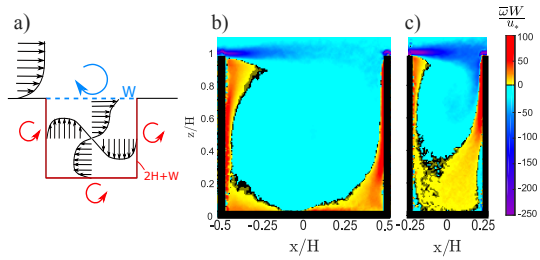

FIGURE 5 a) Qualitative representation of the mean velocity profile inside the cavity and of the vorticity boundary conditions. b-c) Vorticity field inside the cavity for aspect ratios $H/W = 1$ and $H/W = 2$.

vorticity due to flow velocity gradients (first term on the right-hand side), the diffusion of vorticity due to the viscous effects (second term on the right-hand side), and vorticity changes due to thermal gradients (last term of Equation 3). This latter is a source term given by the vector product between the thermal gradient and the gravity vector. Equation 3 is completed by appropriate vorticity conditions at boundaries [e.g., 6, 58]. The main features of these boundary conditions can be grasped by observing the qualitative profile of the mean velocity at the four boundaries of the domain (Figure 5.a). The boundary layer that occurs along the walls of the cavity generates anticlockwise vorticity. Conversely, the shear layer at the top of the cavity generates a Kelvin-Helmholtz type instability leading to the formation of large-scale clockwise vortices that are entrained into the cavity. The same vorticity dynamics in a square cavity-driven flow were observed numerically [15, 66] and experimentally [40, 47] in previous works. To readily understand how the vorticity balance changes in a narrow cavity compared to a square one, a geometry-based interpretation is suggested. Given a constant height H of the canyon, the exchange surface (W) between the external flow and the canyon decreases when the aspect ratio H/W increases. As a consequence, the clockwise vorticity advected inside the cavity decreases as the cavity narrows. The anticlockwise vorticity at walls can be assumed proportional to the solid perimeter of the cavity ($2H + W$). This perimeter also decreases as H/W increases, but less rapidly than W. Consequently, as the aspect ratio increases, a surplus of anticlockwise vorticity accumulates at the bottom of the cavity (Figure 5.c) and a second counter-rotating cell generates.

Note that assuming a change in the aspect ratio from 1 to 2 due to a doubling of H instead of a halving of W, the Reynolds number would double for the narrow cavity. In this case, changes in the vorticity balance due to different flow conditions are expected. Thus, the above presented geometry-based interpretation is valid under the hypothesis of a constant Reynolds number for the two geometries.

After the analysis of the flow field within the cavity, we present below the results about the effect of the canyon geometry on pollutant dispersion. Figure 6 shows the concentration field of the passive scalar released by the ground level source in stationary conditions. The non-dimensional concentration is expressed as $Cu_*H/\dot{M}_q$, where C is the time averaged concentration of ethane, and $\dot{M}_q$ is the mass flow injected at the linear source per unit of length (see Section 2.2). Figure 6.a evidences the presence of a fresh air plume entering the square cavity at the upper corner of the downwind wall. As the aspect ratio of the cavity increases, higher concentrations of pollutants are measured at the pedestrian level compared to the mean concentration in the square cavity. For a cavity with $H/W = 2$ (Figure 6.c), the concentration at street level is up to three times the concentration in the centre of the cavity. Thus, the formation of the second cell inhibits the transfer of pollutants from street level to the external flow, as already found by Hussain and Lee [27], Oke [56], and Jeong and Andrews [30]. Moreover, we observe a different horizontal distribution of the mean concentration at street level in the two

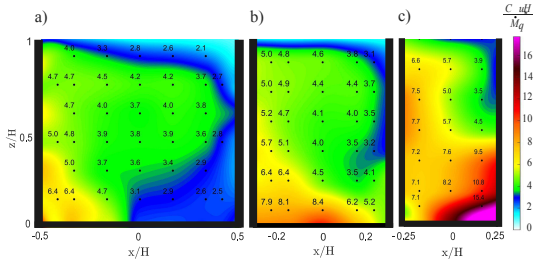

FIGURE 6 Mean concentration of the passive scalar inside the cavity for the aspect ratio (a) $H/W = 1$, (b) $H/W = 1.5$ and (c) $H/W = 2$.

geometries. When the fresh air plume reaches the street level (for H/W=1), pollutant concentration at the lower left corner is double compared to the right corner. Conversely, for H/W=2, 'air quality' is worse at the lower right corner with concentrations that are, also in this case, two times the concentrations measured at the other corner. This spatial distribution of the mean concentration for square and narrow cavities is in accordance with previous studies [5, 4, 41]. In particular, the numerical simulations of Assimakopoulos et al. [4] and Liu et al. [41] showed similar values for the ratio of the concentrations measured in the two lower corners of the cavity.

The above presented results are confirmed by the analysis of the exchange processes inside the canyon for the different geometrical configurations. To this aim, the wash-out curves from the unsteady experiments (see Section 2.2) are considered.

In Figure 7, the wash-out curves measured at different positions for both a square (panel a) and a narrow (panel b) cavity are reported. For each sampling point (points *a* to *e* in the insets in Figure 7), the wash-out curve is normalized by the mean concentration measured at that position in stationary conditions (C_{ss}). We observe that for both geometries all curves have an horizontal tangent for $t \to 0$. As discussed by [63], this feature is not consistent with a one-degree of freedom model, based on the assumption of a perfect mixing within the canyon. In this sense the horizontal tangent indicates an initial mixing process acting on the non-uniform concentrations within the canyon. Moreover, the curves follow two characteristic trends depending on the position of the sampling point. In the square cavity (panel a), the time delay before the concentration decay is longer for the curve registered at the centre of the cavity (point *a*) with respect to those measured in the recirculating part of the flow (points *b*-*e*). The trend of these latter curves is very similar, instead. In the narrow cavity (panel b), the concentration in the upper part of the cavity (points c-e) decays later than in the bottom part of the cavity (points *a*-*b*). The exchange between a street canyon and the atmosphere aloft is traditionally described with box models with one degree of freedom [e.g., 25, 31, 8, 71, 34, 14]. In these simple models, the canyon is described as a box with uniform pollutant concentration and a discontinuity surface at the top, where the exchange takes place. However, the mean concentration field in Figure 6 and the wash-out curves shown in Figure 7 depict a different picture. The mean concentration is far from being uniform within the canyon and the wash-out curves are not identical in all the regions of the flow. These two features evidence how the rate of pollutant transfer is not uniform inside the cavity and that more than one time scale is involved in the wash-out process. Since these experimental data cannot be interpreted with a box model with a single degree of freedom, we apply the analytical model with two degrees of freedom proposed by [61], [63], and [48]. According to this model, the wash-out mechanism is described as a sequence of transfers between three regions,

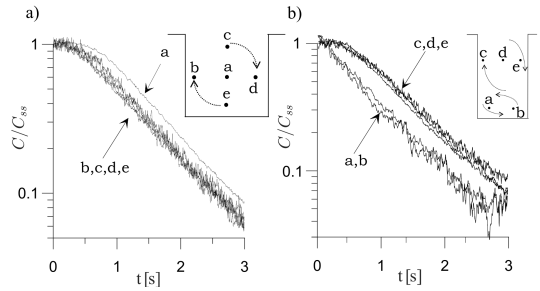

FIGURE 7 Dimensionless wash-out curves measured at different positions within a (a) square cavity with aspect ratio $H/W = 1$ and (b) a narrow cavity with aspect ratio $H/W = 2$.

each one with a different mean concentration (see Figure S1 in the SI). One region represents the external flow, while the two other regions give a rough description of pollutant distribution inside the canyon. In a cavity with a single main recirculating cell (as the square cavity in Figure 7.a), the first region (box_1) is the recirculating part of the flow, while the second region (box_2) is the core of the flow within the main vortex. The distinction between these regions is consistent with the different behaviour observed in Figure 7.a for the the wash-out curve in point *a* with respect to the trend in points *b*-*e*. In a cavity with two recirculating cells (as the narrow cavity in Figure 7.b), the two regions are the cells at the top (box_1) and at the bottom (box_2) of the cavity, in accordance with the two trends observed in Figure 7.b for the concentration measured in points *c*-*e* and *a*-*b*, respectively.

For both a square and a narrow cavity, the model with two degrees of freedom is given by a system of two differential equations (Equation S2 in the SI). This system admits as solution the analytical wash-out curves $C_1(t, u_d, \tilde{u}_d)$ and $C_2(t, u_d, \tilde{u}_d)$ (Equation S9 in the SI) that describe the temporal evolution of the mean concentration in box_1 and box_2 as a function of two free parameters, u_d and $\tilde{u}_d$. The velocity u_d is the bulk exchange velocity between box_1 and the external flow, while $\tilde{u}_d$ is the bulk exchange velocity between box_1 and box_2. The least squared method is applied to find the values of u_d and $\tilde{u}_d$ that minimize the difference between the experimental data and the analytical curves.

In Figure 8, the analytical wash-out curves are compared with the experimental data for a square (panel a) and a narrow cavity (panel b). The good agreement between data and model demonstrates that the simplified two-box model gives a satisfactory description of the cavity wash-out. For both geometries, the estimated velocities u_d and $\tilde{u}_d$ are reported. These results show that, for a narrow cavity, u_d is more than twice $\tilde{u}_d$. The effective transport of pollutant particles from the bottom cell to the upper cell within the cavity is slow, while the wash-out towards the external atmosphere is rapid. Since pollutant release takes place at the pedestrian level, this slower transfer acts as a bottleneck for the entire ventilation process and a higher concentration develops at street level (Figure 6.c). Conversely, in a square cavity, pollutants emitted at street level are directly transferred outside with velocity u_d. In this case, the low $\tilde{u}_d$ value reduces the transfer rate in the centre of the cavity with no significant effects on the street level dynamics.

Since the transition from one to two recirculating cells is crucial for the spatial distribution and the concentration of pollutants inside the cavity, in the following sections we will discuss the effect of wall roughness and heating on this transition.

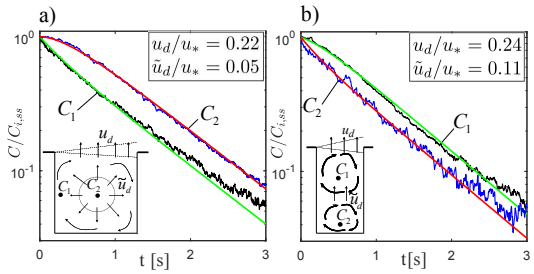

FIGURE 8 a) Experimental (black and blue lines) and analytical (green and red lines) wash-out curves in the recirculating region and in the centre of a square cavity. b) Experimental (black and blue lines) and analytical (green and red lines) wash-out curves at the top and the bottom of a narrow cavity. For both aspect ratios, the wash-out velocities (u_d and $\tilde{u}_d$) are reported.

3.2 | Effect of the small geometrical scale

Experiments with two different roughness scales ($h_r = 2$ mm and $h_r = 5$ mm) at the lateral walls of the canyon were performed. Only the results obtained for roughness elements 5 mm high are shown and discussed here. A similar, but less pronounced, behaviour was observed with small roughness elements.

Figures 2 and 3 evidenced that, for a cavity with smooth walls, the aspect ratio $H/W = 3/2$ is close to the critical ratio for transition. For this geometry, the occurrence of roughness elements (with $h_r = 5$ mm) on the upwind wall of the cavity has slight effects on the mean velocity field (see Figure 9.a compared to Figure 2.b). Conversely, adding roughness to the downwind wall facilitates the formation of the second counter-rotating cell. In fact, the streamlines in Figure 9.b reveal an incipient separation between the regimes of motion in the upper and lower part of the cavity. This behaviour is confirmed for different aspect ratios by the analysis of the vertical profile of the mean horizontal velocity in $x = 0$ (Figure 9.c). With roughness elements on the upwind wall (dashed lines), the vertical profile slightly differs from the profile that is established in the cavity with smooth walls (dotted lines). With roughness on the downwind wall (continuous line) the vertical profile tends to the characteristic profile of a motion with two counter-rotating cells, as those observed in Figure 3 for aspect ratios greater than 1.8.

As for the large geometrical scale, the effect of wall roughness can be interpreted in terms of vorticity. Wall roughness increases the mean velocity gradients near the walls. As a consequence, the vorticity flux from the wall towards the cavity (Figure 5.a) is enhanced. However, for a rough upwind wall, the additional anticlockwise vorticity is more rapidly transferred outside the cavity, so that it does not significantly modify the vorticity balance in the domain. This is evidenced by panels d and e in Figure 9 showing the vorticity field in a cavity with aspect ratio 3/2 with smooth walls and with roughness elements on the upwind wall, respectively. On the other hand, the additional anticlockwise vorticity generated at the rough downwind wall is advected along the streamlines of the mean velocity field in the core of the cavity, where it induces the formation of the counter-rotating cell. The increase in anticlockwise vorticity at the bottom of the cavity can be observed in the case of roughness elements on the downwind wall in Figure 9.f.

The formation of secondary vortices in the street canyon due to the presence of roughness elements on building walls is confirmed by the numerical studies of Murena and Mele [49] and Llaguno-Munitxa et al. [42], who observed a reduced turbulence intensity and a slower wash-out of the cavity. However, these numerical studies did not analyse the effect of roughness on one wall at a time.

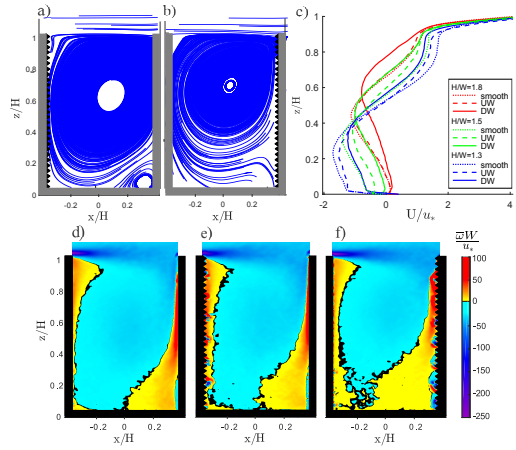

FIGURE 9 Effect on the mean velocity field of wall roughness at the (a) upwind (UW) and (b) downwind (DW) wall for a cavity with $H/W = 3/2$. (c) Vertical profile of the mean horizontal velocity in $x = 0$ for different aspect ratios and for different conditions of the walls: smooth walls (dotted lines), UW roughness (dashed lines) and DW roughness (continuous lines). Normalized vorticity field within a cavity with H/W=3/2 and with (a) smooth walls, (b) UW wall roughness, (c) DW wall roughness.

4 | EFFECT OF WALL HEATING

4.1 | Effect of upwind wall heating

The upwind wall of the cavity is heated and three temperature differences (ΔT) are experimented and discussed: 0 K, 140 K, and 240 K (Froude numbers are reported in Table 1). The effect of wall heating is investigated for a square cavity ($H/W = 1$) and for a narrow cavity with an aspect ratio $H/W = 3/2$. As observed in the previous sections, in this latter geometrical configuration the flow field is close to the transition from one to two recirculating cells.

Regardless the wall temperature, the mean velocity profiles (panels a and b in Figure 10) evidence the presence of a shear layer at the cavity top, where the vertical profile of the horizontal component (black lines) reaches its maximum. The level of TKE (panels c and d in Figure 10) is higher at the cavity top and along the downwind wall, where a TKE plume spreads down in the cavity from the external flow.

We observe negligible variations in the mean and fluctuating velocity fields, when the upwind wall is heated. This is found for both a square (panels a and c in Figure 10) and a narrow (panels b and d Figure 10) cavity. Other authors [e.g., 3, 44] found a slight increase of the mean motion and of the TKE inside a square cavity due to buoyancy effects at the upwind wall. This is likely to be due to the lower internal Froude number considered in their experiments, that, as mentioned in Section 2.3, is one order of magnitude lower than the Fr_i values experimented here.

4.2 | Effect of downwind wall heating

The downwind wall of the cavity is heated and four temperature differences (ΔT) are considered: 0 K, 70 K, 170 K and 240 K (Froude numbers are reported in Table 1). When the downwind wall is heated, we observe

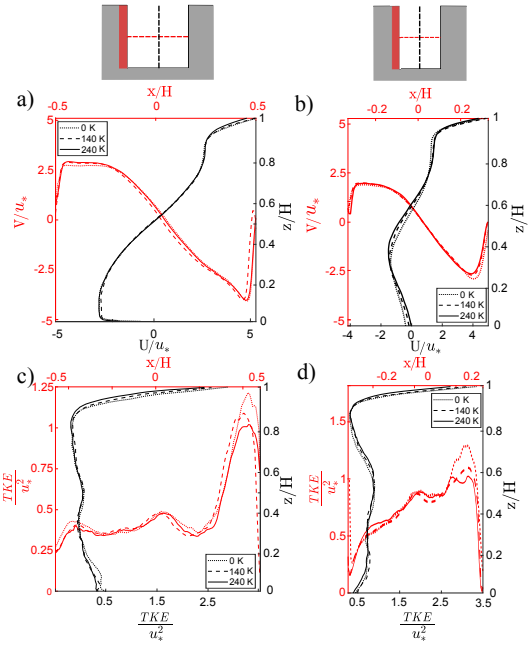

FIGURE 10 Upwind wall heating. Horizontal (red lines) and vertical (black lines) profiles of the vertical (V) and horizontal (U) components of the mean velocity (panels a and b) and of the TKE (panels c and d) within the cavity for the aspect ratios $H/W = 1$ (left panels) and 1.5 (right panels).

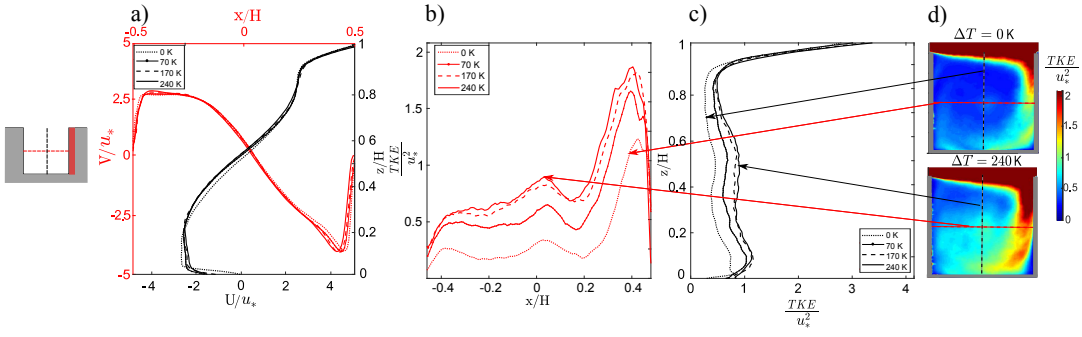

FIGURE 11 Downwind wall heating for a square cavity ($H/W = 1$). Horizontal (red lines) and vertical (black lines) profiles of the vertical (V) and horizontal (U) components of the mean velocity (a) and of the TKE inside the cavity (b and c). In d, the TKE field for the maximum heating configuration is compared to the configuration with no heated walls.

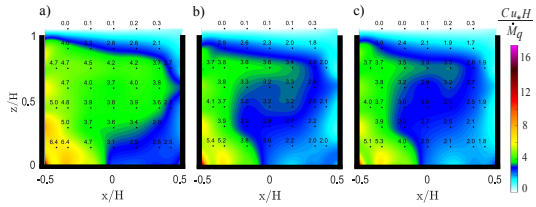

FIGURE 12 Concentration of a passive scalar released at street level in a square cavity for different heating of the downwind wall: (a) $\Delta T = 0$ K, (b) $\Delta T = 70$ K, and (c) $\Delta T = 170$ K.

diverse effects depending on the aspect ratio of the cavity.

For square cavities ($H/W = 1$), in the range of Fr_i considered in this study, the heating of the downwind wall has negligible effects on the mean velocity field. Figure 11.a shows the vertical profile of the mean horizontal velocity (U) and the horizontal profile of the vertical velocity component (V). The profiles at different temperature configurations tend to overlap. In the SI, more results about the mean vertical velocity field for these configurations are reported. The heating of the downwind wall has evident effects on the fluctuating field, instead. An increment of around 400% and 200% is observed for the horizontal (Figure 11.b) and vertical (Figure 11.c) profiles of the TKE when ΔT increases from 0 to 240 K. These variations are significantly higher than the error associated to the estimate of the TKE by means of PIV (see Section 2.2). Even for the TKE variations measured for ΔT =70 K and 170 K, the measurement error is negligible. While the variation from ΔT =170 K to 240 K is subject to the greatest degree of uncertainty. For a square cavity, this increase in the turbulent fluctuations near the heated downwind wall is confirmed by the studies of Allegrini et al. [3] and Marucci and Carpentieri [44]. However, with respect to our findings, they also observed a different mean flow structure with the formation of a secondary rotating vortex, due to the lower values of Fr_i imposed in their experiments.

The mean concentration of pollutants inside the cavity decreases with increasing ΔT when $H/W = 1$ (Figure 12). This suggests a more efficient canyon ventilation. To further explore this behaviour, as customary, we turn to the analysis of the wash-out curves provided by the unsteady experiments. In Figure 13, the concentration in both the lateral (panel a) and central (panel b) part of the cavity decays more rapidly as the thermal flux at the downwind wall is increased. The wash-out velocities (Table 2), estimated by the application of the model with two degrees of freedom, reveal that the heating of the downwind wall enhances the wash-out velocities, $\tilde{u}_d$ and u_d. Notice that the results for $\Delta T = 240$ K are here not reported as the experiments in unsteady conditions for this configuration were not performed.

Thus, for a square cavity, the heating of the downwind wall increases the levels of TKE within the cavity and enhances the canyon ventilation, while the mean motion is almost unaltered. Moreover, the values of the estimated wash-out velocities (u_d and $\tilde{u}_d$) are very low compared to the characteristic velocity scale for the mean advection in the cavity. These findings are in accordance with previous works [63] suggesting that the cavity wash-out, in a perpendicular street canyon, is mainly regulated by the fluctuating component of the velocity field. These considerations will be discussed in detail in Section 5.

In narrow cavities ($H/W = 1.5$), the heating of the downwind wall has remarkable effects on both the mean motion (panels a to c in Figure 14) and the TKE inside the cavity (panels d to g in Figure 14). The thermal

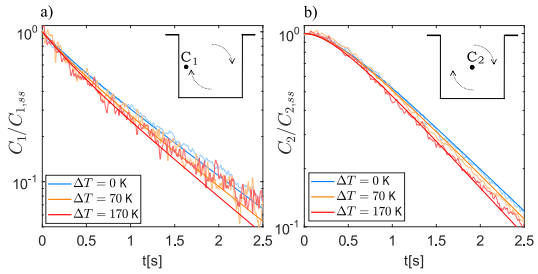

FIGURE 13 Dimensionless wash-out curves measured in the (a) lateral and (b) central part of a square cavity for different heating of the downwind wall. The analytical wash-out curves are above the experimental data (shaded lines).

TABLE 2 Variation of the wash-out velocities (u_d and $\tilde{u}_d$) as a function of the temperature difference ΔT in a square cavity.

	ΔT = 0 K	ΔT = 70 K	ΔT = 170 K
	$Fr_i = \infty$	Fr_i = 0.62	Fr_i = 0.40
u_d/u_* [-]	0.22	0.33	0.35
$\tilde{u}_d/u_*$ [-]	0.050	0.066	0.069

gradient near the downwind wall facilitates the transition from one cell to two counter-rotating cells (panel c). This behaviour is evidenced by the vertical profile of the mean horizontal velocity in $x = 0$ (panel b) that tends to the characteristic profile of a motion with two counter-rotating cells as ΔT increases and Fr_i decreases (see the cases of $H/W \geq 1.8$ in Figure 3). As seen in Figure 4, this transition inhibits the penetration of the TKE plume from the external flow into the cavity. Thus, the highest values of TKE at street level are reached for the no-heated configuration (dotted line in Figure 14.e): as the temperature of the wall increases, the level of TKE enhances in the upper part of the canyon (panel d) while a low turbulence region develops at street level (panel e). As pointed out for the square cavity, the uncertainty in TKE measurements by means of PIV does not compromise the reliability of the observed trends.

In this configuration, the role of TKE on canyon ventilation, compared to the role of advection, can hardly be distinguished. Here, the topology of the mean flow has an evident effect on the distribution of the TKE and thus on canyon ventilation. However, the role of TKE in the pollutant transfer (found above for a square cavity) is in accordance with the results obtained here for a narrow cavity. The enhancement of the turbulent fluctuations in the upper part of the cavity (Figure 14.d) accelerates wash-out of pollutants at roof level, while the decreasing TKE levels in the bottom part of the cavity (Figure 14.e) inhibits the vertical transfer of pollutants from street level. Since the pollutant source is placed at street level, the slowing down of the transfer in the lower part of the cavity acts as a bottleneck for the entire ventilation process and thus, in steady conditions, the concentration of pollutants at street level increases with the temperature of the downwind wall (Figure 15.c). In the SI, we further discuss the possible role of the mean motion (compared to the TKE) in canyon ventilation.

As shown for the square cavity (see Figure 13 and Table 2), the analysis of the wash-out process would

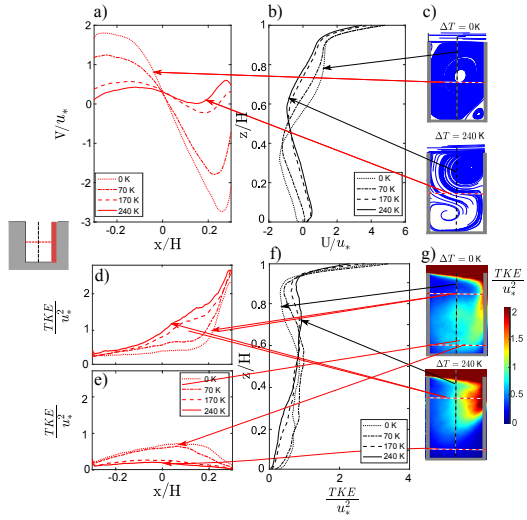

FIGURE 14 Downwind wall heating for a narrow cavity ($H/W = 1.5$). Horizontal (red lines) and vertical (black lines) profiles of the vertical (V) and horizontal (U) components of the mean velocity (a and b) and of the TKE (d to e) inside the cavity. In panels c and g, the mean velocity field and the TKE field for the configuration with $\Delta T = 240$ K is compared to the configuration with $\Delta T = 0$ K.

provide further insights into the transport mechanisms. However, for the cavity with $H/W = 1.5$ the analytical model for the wash-out process is not useful for comparing the different configurations. In fact, for $\Delta T = 0$ K, the model for a square cavity should be applied since a single vortex establishes in the cavity (see panel c in Figure 14). For $\Delta T = 170$ K, two distinct vortices can be identified and thus the model with two boxes connected in series has to be used. In the transition ($\Delta T = 70$ K) neither of the two models is applicable since we cannot clearly identify the spatial extent of the two cells.

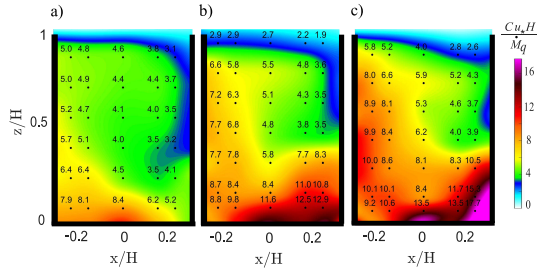

FIGURE 15 Concentration of a passive scalar released at street level in a narrow cavity for different heating of the downwind wall: a) $\Delta T = 0$ K, b) $\Delta T = 70$ K, and c) $\Delta T = 170$ K

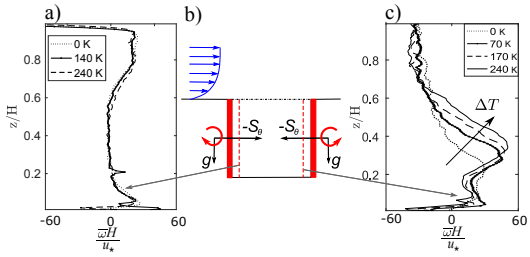

FIGURE 16 Schematic representation of the vorticity generation near the heated walls (b). Vertical profile of the vorticity near the upwind (a) and downwind (b) walls for a square cavity in the case of upwind wall heating and downwind wall heating, respectively.

4.3 | Vorticity dynamics in a heated cavity

As for the role of aspect ratio and wall roughness (Section 3), the analysis of the vorticity dynamics within the cavity helps in clarifying the different flow behaviours observed for the heating of the upwind and downwind wall (Sections 4.1-4.2).

In the vorticity transport equation (Equation 3), the last term accounts for vorticity production due to thermal gradients. When the upwind wall is heated, the vector product between the opposite of the thermal gradient S_T and the gravity vector generates clockwise vorticity near the wall (Figure 16.b). This additional vorticity is in accordance with the main vorticity field inside the cavity and, due to geometrical reasons, it is rapidly transferred outside the cavity with negligible effects on the mean and fluctuating velocity components. Indeed, the vorticity near the upwind heated wall in a square cavity (Figure 16.a) exhibits a vertical profile with negligible variations for different buoyancy conditions.

Conversely, when the downwind wall is heated, the thermal gradient generates anticlockwise vorticity near the wall (Figure 16.b). Figure 16.c evidences a trend toward positive and thus anticlockwise vorticity near the downwind heated wall of a square cavity. Similarly to the case of a rough downwind wall (section 3.2), the additional anticlockwise vorticity generated at the wall is advected in the core of the flow field. For a square cavity, this additional anticlockwise vorticity seems to only affect the fluctuating velocity field (Figure 11b-d), while, in a narrow cavity, it triggers the formation of the second cell (Figure 14a-c).

5 | TURBULENT KINETIC ENERGY AND CANYON VENTILATION

The experimental results reported in Section 4.2 suggest a correlation between the increase in turbulent kinetic energy and the velocity of the wash-out process in an idealised 2D street canyon perpendicular to the wind direction. In the square cavity, TKE levels enhance within the entire cavity due to the heating of the downwind wall. At the same time, an acceleration is observed in the pollutant exchange between the cavity and the external atmosphere (u_d), and between the core and the outer part of the recirculating cell within the cavity ($\tilde{u}_d$). In the narrow cavity instead, thermal fluxes at the downwind wall induce the formation of two counter-rotating cells, and thus the TKE increases at the top of the cavity but decreases at street level. The results for the concentration field suggest that the vertical exchange at roof level (u_d) is accelerated, while the exchange between the two internal cells ($\tilde{u}_d$) is inhibited.

Our interpretation for this higher efficiency of the turbulent transport in the ventilation of the perpendicular

canyon is that this mechanism is responsible for the transfer of pollutant particles across the streamlines of the flow, in a dispersive motion that actually allows the particles to be intercepted by the shear layer at the roof top and brought outside the cavity. This interpretation is in line with the analysis of Salizzoni et al. [63]. In this previous work, the wash-out time varied with the intensity of the turbulent fluctuations within the cavity, induced in turn by a variation of the flow statistics of the external flow. Here, we are instead keeping the external flow unaltered but we are modifying the conditions within the cavity.

In lights of the present experimental results and of the analysis proposed in [63], we further investigate in this Section the dependency of the wash-out velocity on the fluctuating component of the turbulent flow. To this aim, we first estimate the velocities u_d and $\tilde{u}_d$ for all the experimental configurations in which the model with two degrees of freedom can be applied, i.e. the configurations in which only one or two vortices are clearly established in the cavity. These include the experiments in a square cavity with different heat fluxes at the downwind wall (cases 1 to 3 in Figure 17), and the case of an isothermal cavity with aspect ratio $H/W = 2$ (case 7). For $H/W = 3/2$, we consider the configurations with $\Delta T = 0$ K (the flow field has a single-vortex structure), $\Delta T = 140$ K and $\Delta T = 170$ K (the flow field has a two-vortex structure). These are cases 4 to 6 in Figure 17. Other configurations are not considered as, in case of transition from one to two vortices, the model with two degrees of freedom fails to describe adequately the wash-out process.

Velocities u_d and $\tilde{u}_d$ are plotted against TKE levels inside the cavity. In particular, since each velocity describes the rate of pollutant transfer out of a specific region of the cavity (box_1 and box_2 in Figure S1 in the SI), we calculate for each one of these regions the spatial average of the TKE from PIV data. In Figure 17, the spatially averaged TKE for each region is plotted against the corresponding wash-out velocity. For each configuration (numbers 1 to 7), the blue and orange markers report the results for box_1 and box_2, respectively. The error bars represent the uncertainty of the results associated with the two parameters γ and β of the wash-out model (see Section S1 in the SI). As expected, results show a positive correlation between TKE and the wash-out velocity. Interestingly, a clear linear relationship can be observed for u_d (blue markers), i.e. for the velocity characterizing the exchange at the roof level. The interpretation of the behaviour of $\tilde{u}_d$ (orange markers) is less straightforward. For configurations with a single main vortex (1 to 4) the internal exchange velocity slowly grows with TKE. In configurations with two counter-rotating vortices (5-7), the non-dimensional exchange velocity $\tilde{u}_d$ is larger than in single-vortex configurations. A dependence with the local TKE levels is however less easy to enlighten, also due to the non-negligible extent of the error bars, the limited number (only three) of data points available in the present analysis, and the lack of a perfect two-dimensionality of the flow in the lower cell. The existence of different trends of $\tilde{u}_d$ as a function of u_* further suggests that (differently from the case of u_d) this exchange process may be affected by the topology of the mean flow. Enlightening this feature would require a more in-depth analysis of the transport mechanisms and further measurements in a wider range of flow conditions. In general, the measurement of the turbulent pollutant fluxes, as well as the analysis of the spatial distribution of the concentration fluctuations within the cavity, could further clarify the role of TKE in the mechanisms driving cavity ventilation and the wash-out of pollutants.

6 | CONCLUSIONS

We have investigated the vertical exchange of pollutants between a street canyon and the external flow. We have considered the case of a wind blowing perpendicular to the axis of the street. To grasp the physical mechanisms that govern the canyon ventilation, we have performed multiple wind tunnel experiments covering

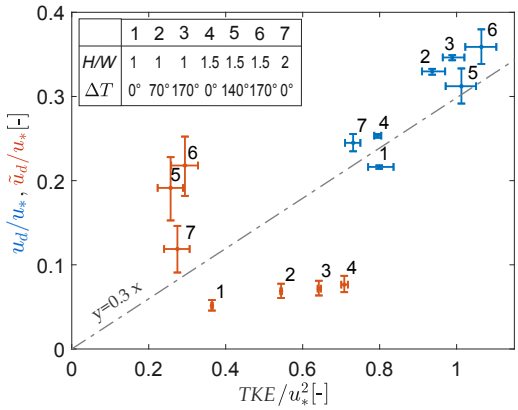

FIGURE 17 Wash-out velocity u_d (blue markers) and $\tilde{u}_d$ (orange markers) against the mean TKE in the corresponding region. Numbers 1-7 indicates the different experimental configurations. The dash-dotted line is the result of a linear regression through the origin of all the points shown in the chart.

a wide range of street canyon configurations. In particular, different canyon geometries and thermal conditions at walls have been analysed.

In accordance with previous works, results have evidenced that the transition of the mean velocity field within the cavity from one to two recirculating cells strongly influences the vertical removal of pollutants. The wind tunnel experiments showed that the occurrence of this transition depends on different properties of the street canyon.

As the aspect ratio of the cavity increases, the total anticlockwise vorticity fluxes at the cavity walls increase as well. This feature induces the formation of the second counter-rotating cell, thus hindering the canyon ventilation. As a consequence, in narrow canyons air quality at the pedestrian level is worsened.

Wall roughness enhances velocity gradients near the walls, inducing higher fluxes of anticlockwise vorticity. Adding roughness to the downwind wall facilitates the transition to two recirculating cells, while roughness elements at the upwind wall slightly influence the velocity field since the enhanced anti-clockwise vorticity is rapidly advected outside the cavity by the mean motion.

Thermal fluxes at the upwind wall have negligible effects on both the mean and TKE fields. Similarly to wall roughness, the heating of the upwind wall produces clockwise vorticity that is transferred outside the cavity before affecting the flow.

From the environmental point of view, the heating of the downwind wall has opposite effects depending on the street aspect ratio. In a square cavity, the thermal fluxes are not strong enough to modify the topology of the mean flow streamlines, but their effect is relevant on the intensity of the TKE, which is increased in the whole cavity. This increase in TKE seems to be associated to the acceleration of the wash-out from the canyon to the overlying atmospheric flow, with a resulting reduction of the passive scalar concentration within the canyon. As the aspect ratio of the cavity increases, the heating of the downwind wall has growing effects on the velocity field. For $H/W = 1.5$, the heating of the wall facilitates the formation of the second cell at the bottom of the canyon, thus slowing down the wash-out process. As a consequence, pollutants accumulate at street level with consequent deterioration of air quality.

These results bring together findings from previous works which investigated the effect of single factors on

the velocity and concentration field inside a street canyon. The comprehensive analysis of multiple configurations involving different physical aspects (geometry, roughness, heating) displays how the different parameters interact, and traces a link between the acceleration in the wash-out process and the increase in the TKE levels, in accordance with the analysis of Salizzoni et al. [63].

However, further experimental studies are desirable. In particular, measurements of the turbulent and mean components of the vertical pollutant fluxes would be helpful to clarify the role of TKE in the canyon ventilation. We finally stress that the experimental results presented in this work are valid for an idealised 2D street canyon with a perpendicular orientation with respect to the wind direction. However, this dataset is valuable in validating numerical simulations in two-dimensional canyons, and in reducing uncertainties in modelling the effects of the street canyon aspect ratio, wall roughness and temperature of façades on the flow and concentration field within a street.

7 | ACKNOWLEDGEMENTS

This study was supported by the Italian-French/French-Italian University via the Vinci Program, and by the Région Auvergne Rhône-Alpes via the SCUSI Projetc. Moreover, we would like to express our gratitude to Patrick Mejean and Nathalie Grosjean for the technical support in performing the wind tunnel experiments.

references

[1] Adrian, R., 1997. Dynamic ranges of velocity and spatial resolution of particle image velocimetry. Measurement Science and Technology 8 (12), 1393.

[2] Alexandri, E., Jones, P., 2008. Temperature decreases in an urban canyon due to green walls and green roofs in diverse climates. Building and environment 43 (4), 480–493.

[3] Allegrini, J., Dorer, V., Carmeliet, J., 2013. Wind tunnel measurements of buoyant flows in street canyons. Building and Environment 59, 315–326.

[4] Assimakopoulos, V. D., ApSimon, H., Moussiopoulos, N., 2003. A numerical study of atmospheric pollutant dispersion in different two-dimensional street canyon configurations. Atmospheric Environment 37 (29), 4037–4049.

[5] Baik, J.-J., Kim, J.-J., 1999. A numerical study of flow and pollutant dispersion characteristics in urban street canyons. Journal of applied meteorology 38 (11), 1576–1589.

[6] Banerjee, T., Katul, G., Fontan, S., Poggi, D., Kumar, M., 2013. Mean flow near edges and within cavities situated inside dense canopies. Boundary-layer meteorology 149 (1), 19–41.

[7] Barlow, J. F., Belcher, S. E., 2002. A wind tunnel model for quantifying fluxes in the urban boundary layer. Boundary-Layer Meteorology 104 (1), 131–150.

[8] Berkowicz, R., 2000. Ospm-a parameterised street pollution model. Environmental monitoring and assessment 65 (1-2), 323–331.

[9] Bibri, S. E., Krogstie, J., 2017. Smart sustainable cities of the future: An extensive interdisciplinary literature review. Sustainable Cities and Society 31, 183–212.

[10] Bozovic, R., Maksimovic, C., Mijic, A., Smith, K., Suter, I., Van Reeuwijk, M., 2017. Blue green solutions. a systems approach to sustainable and cost-effective urban development.

[11] Cai, X.-M., 2012. Effects of wall heating on flow characteristics in a street canyon. Boundary-layer meteorology 142 (3), 443–467.

[12] Carpentieri, M., Hayden, P., Robins, A. G., 2012. Wind tunnel measurements of pollutant turbulent fluxes in urban intersections. Atmospheric Environment 46, 669–674.

[13] Castro, I., Robins, A., 1977. The flow around a surface-mounted cube in uniform and turbulent streams. Journal of fluid Mechanics 79 (2), 307–335.

[14] Caton, F., Britter, R., Dalziel, S., 2003. Dispersion mechanisms in a street canyon. Atmospheric Environment 37 (5), 693–702.

[15] Chang, K., Constantinescu, G., Park, S.-o., 2006. Analysis of the flow and mass transfer processes for the incompressible flow past an open cavity with a laminar and a fully turbulent incoming boundary layer. Journal of Fluid Mechanics 561, 113–145.

[16] Cui, Z., Cai, X., J Baker, C., 2004. Large-eddy simulation of turbulent flow in a street canyon. Quarterly Journal of the Royal Meteorological Society 130 (599), 1373–1394.

[17] Fackrell, J., 1980. A flame ionisation detector for measuring fluctuating concentration. Journal of Physics E: Scientific Instruments 13 (8), 888.

[18] Fellini, S., Salizzoni, P., Soulhac, L., Ridolfi, L., 2019. Propagation of toxic substances in the urban atmosphere: A complex network perspective. Atmospheric Environment 198, 291–301.

[19] Georgakis, C., Santamouris, M., 2006. Experimental investigation of air flow and temperature distribution in deep urban canyons for natural ventilation purposes. Energy and buildings 38 (4), 367–376.

[20] Gromke, C., Ruck, B., 2007. Influence of trees on the dispersion of pollutants in an urban street canyon - Experimental investigation of the flow and concentration field. Atmospheric Environment 41 (16), 3287–3302.

[21] Haaland, C., van den Bosch, C. K., 2015. Challenges and strategies for urban green-space planning in cities undergoing densification: A review. Urban forestry & urban greening 14 (4), 760–771.

[22] Harman, I., Belcher, S., 2006. The surface energy balance and boundary layer over urban street canyons. Quarterly Journal of the Royal Meteorological Society 132 (621), 2749–2768.

[23] Heilig, G. K., 2012. World urbanization prospects: the 2011 revision. United Nations, Department of Economic and Social Affairs (DESA), Population Division, Population Estimates and Projections Section, New York 14.

[24] Hertel, O., De Leeuw, F. A., Jensen, S. S., Gee, D., Herbarth, O., Pryor, S., Palmgren, F., Olsen, E., et al., 2001. Human exposure to outdoor air pollution (IUPAC technical report). Pure and Applied Chemistry 73 (6), 933–958.

[25] Hotchkiss, R. S., 1973. Air pollution transport in street canyons. Prepared for EPA.

[26] Hunt, G., Linden, P., 1999. The fluid mechanics of natural ventilation—displacement ventilation by buoyancy-driven flows assisted by wind. Building and Environment 34 (6), 707–720.

[27] Hussain, M., Lee, B. E., 1980. A wind tunnel study of the mean pressure forces acting on large groups oflow-rise buildings 6, 207–225.

[28] Hyun, B., Balachandar, R., Yu, K., Patel, V., 2003. Assessment of piv to measure mean velocity and turbulence in open-channel flow. Experiments in Fluids 35 (3), 262–267.

[29] Irwin, H., 1981. The design of spires for wind simulation. Journal of Wind Engineering and Industrial Aerodynamics 7 (3), 361 – 366.

[30] Jeong, S. J., Andrews, M. J., 2002. Application of the k–ε turbulence model to the high Reynolds number skimming flow field of an urban street canyon. Atmospheric environment 36 (7), 1137–1145.

[31] Johnson, W., Ludwig, F., Dabberdt, W., Allen, R., 1973. An urban diffusion simulation model for carbon monoxide. Journal of the Air Pollution Control Association 23 (6), 490–498.

[32] Kim, J.-J., Baik, J.-J., 2001. Urban street-canyon flows with bottom heating. Atmospheric Environment 35 (20), 3395–3404.

[33] Kovar-Panskus, A., Moulinneuf, L., Savory, E., Abdelqari, A., Sini, J.-F., Rosant, J.-M., Robins, A., Toy, N., 2002. A wind tunnel investigation of the influence of solar-induced wall-heating on the flow regime within a simulated urban street canyon. Water, Air and Soil Pollution: Focus 2 (5-6), 555–571.

[34] Kukkonen, J., Valkonen, E., Walden, J., Koskentalo, T., Aarnio, P., Karppinen, A., Berkowicz, R., Kartastenpää, R., 2001. A measurement campaign in a street canyon in Helsinki and comparison of results with predictions of the ospm model. Atmospheric Environment 35 (2), 231–243.

[35] Lee, I. Y., Park, H. M., 1994. Parameterization of the pollutant transport and dispersion in urban street canyons. 28 (14), 2343–2349.

[36] Lee, S.-H., Lee, H., Park, S.-B., Woo, J.-W., Lee, D.-I., Baik, J.-J., 2016. Impacts of in-canyon vegetation and canyon aspect ratio on the thermal environment of street canyons: numerical investigation using a coupled WRF-VUCM model. Quarterly Journal of the Royal Meteorological Society 142 (699), 2562–2578.

[37] Leonardi, S., Orlandi, P., Antonia, R. A., 2007. Properties of d-and k-type roughness in a turbulent channel flow. Physics of fluids 19 (12), 125101.

[38] Li, X.-X., Britter, R., Norford, L. K., 2016. Effect of stable stratification on dispersion within urban street canyons: A large-eddy simulation. Atmospheric environment 144, 47–59.

[39] Li, X.-X., Britter, R. E., Norford, L. K., Koh, T.-Y., Entekhabi, D., 2012. Flow and pollutant transport in urban street canyons of different aspect ratios with ground heating: large-eddy simulation. Boundary-layer meteorology 142 (2), 289–304.

[40] Lin, J.-C., Rockwell, D., 2001. Organized oscillations of initially turbulent flow past a cavity. Aiaa Journal 39 (6), 1139–1151.

[41] Liu, C.-H., Barth, M. C., Leung, D. Y., 2004. Large-eddy simulation of flow and pollutant transport in street canyons of different building-height-to-street-width ratios. Journal of Applied Meteorology 43 (10), 1410–1424.

[42] Llaguno-Munitxa, M., Bou-Zeid, E., Hultmark, M., 2017. The influence of building geometry on street canyon air flow: Validation of large eddy simulations against wind tunnel experiments. Journal of Wind Engineering and Industrial Aerodynamics 165, 115–130.

[43] Louka, P., Vachon, G., Sini, J.-F., Mestayer, P., Rosant, J.-M., 2002. Thermal effects on the airflow in a street canyon - Nantes' 99 experimental results and model simulations. Water, air and soil pollution: Focus 2 (5-6), 351–364.

[44] Marucci, D., Carpentieri, M., 2019. Effect of local and upwind stratification on flow and dispersion inside and above a bi-dimensional street canyon. Building and Environment 156, 74–88.

[45] Mehta, U. B., Lavan, Z., 1969. Flow in a two dimensional channel with a rectangular cavity. Journal of Applied Mechanics 36, 897–901.

[46] Meroney, R. N., Pavageau, M., Rafailidis, S., Schatzmann, M., 1996. Study of line source characteristics for 2-d physical modelling of pollutant dispersion in street canyons. Journal of wind Engineering and industrial Aerodynamics 62 (1), 37–56.

694 [47] Mori, T., Naganuma, K., 2009. Experimental investigation of the three-dimensional nature of turbulent flow
695 over a rectangular cavity. Journal of Fluid Science and Technology 4 (3), 746–757.

696 [48] Murena, F., Di Benedetto, A., D'Onofrio, M., Vitiello, G., 2011. Mass transfer velocity and momentum vertical
697 exchange in simulated deep street canyons. Boundary-layer meteorology 140 (1), 125.

698 [49] Murena, F., Mele, B., 2016. Effect of balconies on air quality in deep street canyons. Atmospheric Pollution
699 Research 7 (6), 1004–1012.

700 [50] Nakamura, Y., Oke, T. R., 1988. Wind, temperature and stability conditions in an east-west oriented urban
701 canyon. Atmospheric Environment (1967) 22 (12), 2691–2700.

702 [51] Nazarian, N., Martilli, A., Kleissl, J., 2018. Impacts of realistic urban heating, part I: spatial variability of mean
703 flow, turbulent exchange and pollutant dispersion. Boundary-layer meteorology 166 (3), 367–393.

704 [52] Niachou, K., Livada, I., Santamouris, M., 2008. Experimental study of temperature and airflow distribution
705 inside an urban street canyon during hot summer weather conditions. part II: Airflow analysis. Building and
706 environment 43 (8), 1393–1403.

707 [53] Nironi, C., 2013. Concentration fluctuations of a passive scalar in a turbulent boundary layer. Ph.D. thesis.

708 [54] Nironi, C., Salizzoni, P., Marro, M., Mejean, P., Grosjean, N., Soulhac, L., 2015. Dispersion of a passive scalar
709 fluctuating plume in a turbulent boundary layer. part i: Velocity and concentration measurements. Boundary-
710 layer meteorology 156 (3), 415–446.

711 [55] Offerle, B., Eliasson, I., Grimmond, C., Holmer, B., 2007. Surface heating in relation to air temperature, wind
712 and turbulence in an urban street canyon. Boundary-Layer Meteorology 122 (2), 273–292.

713 [56] Oke, T. R., 1988. Street design and urban canopy layer climate. Energy and Buildings 11, 103–113.

714 [57] Oke, T. R., 2002. Boundary layer climates. Routledge.

715 [58] Olshanskii, M. A., Heister, T., Rebholz, L. G., Galvin, K. J., 2015. Natural vorticity boundary conditions on
716 solid walls. Computer Methods in Applied Mechanics and Engineering 297, 18–37.

717 [59] Pavageau, M., Schatzmann, M., 1999. Wind tunnel measurements of concentration fluctuations in an urban
718 street canyon. Atmospheric Environment 33 (24-25), 3961–3971.

719 [60] Prasad, A. K., 2000. Particle image velocimetry. Current Science-Bangalore- 79 (1), 51–60.

720 [61] Salizzoni, P., 2006. Mass and momentum transfer in the urban boundary layer. Ph.D. thesis, Ecully, Ecole
721 centrale de Lyon.

722 [62] Salizzoni, P., Marro, M., Soulhac, L., Grosjean, N., Perkins, R. J., 2011. Turbulent transfer between street
723 canyons and the overlying atmospheric boundary layer. Boundary-layer meteorology 141 (3), 393–414.

724 [63] Salizzoni, P., Soulhac, L., Mejean, P., 2009. Street canyon ventilation and atmospheric turbulence. Atmospheric
725 Environment 43 (32), 5056–5067.

726 [64] Salizzoni, P., Soulhac, L., Mejean, P., Perkins, R. J., 2008. Influence of a two-scale surface roughness on a
727 neutral turbulent boundary layer. Boundary-layer meteorology 127 (1), 97–110.

728 [65] Santamouris, M., Papanikolaou, N., Livada, I., Koronakis, I., Georgakis, C., Argiriou, A., Assimakopoulos, D.,
729 2001. On the impact of urban climate on the energy consumption of buildings. Solar energy 70 (3), 201–216.

730 [66] Shi, L., Wang, Y., Jin, Y., Zhang, G., Zhang, D., 2019. Parametrical study and turbulence analysis of high-speed
731 flows around an open cavity using large eddy simulation. Fluid Dynamics Research 51 (3), 035503.

[67] Sini, J.-F., Anquetin, S., Mestayer, P. G., 1996. Pollutant dispersion and thermal effects in urban street canyons. Atmospheric environment 30 (15), 2659–2677.

[68] Snyder, W., 1994. Some observations of the influence of stratification on diffusion in building wakes. In: Castro, I., Rockliff, N. (Eds.), Stably Stratified Flows and Dispersion over Topography. Claredon Press, pp. 301–324.

[69] Solazzo, E., Britter, R., 2007. Transfer processes in a simulated urban street canyon. Boundary-Layer Meteorology 124 (1), 43–60.

[70] Solazzo, E., Cai, X., Vardoulakis, S., 2008. Modelling wind flow and vehicle-induced turbulence in urban streets. Atmospheric Environment 42 (20), 4918–4931.

[71] Soulhac, L., 2000. Modélisation de la dispersion atmosphérique à l'intérieur de la canopée urbaine. Ph.D. thesis, Ecole Centrale de Lyon.

[72] Soulhac, L., Nguyen, C. V., Volta, P., Salizzoni, P., 2017. The model sirane for atmospheric urban pollutant dispersion. part iii: Validation against no2 yearly concentration measurements in a large urban agglomeration. Atmospheric environment 167, 377–388.

[73] Soulhac, L., Salizzoni, P., 2010. Dispersion in a street canyon for a wind direction parallel to the street axis. Journal of Wind Engineering and Industrial Aerodynamics 98 (12), 903–910.

[74] Soulhac, L., Salizzoni, P., Cierco, F.-X., Perkins, R., 2011. The model sirane for atmospheric urban pollutant dispersion; part i, presentation of the model. Atmospheric environment 45 (39), 7379–7395.

[75] Soulhac, L., Salizzoni, P., Mejean, P., Didier, D., Rios, I., 2012. The model sirane for atmospheric urban pollutant dispersion; part ii, validation of the model on a real case study. Atmospheric environment 49, 320–337.

[76] Theeuwes, N., Steeneveld, G., Ronda, R., Heusinkveld, B., Van Hove, L., Holtslag, A., 2014. Seasonal dependence of the urban heat island on the street canyon aspect ratio. Quarterly Journal of the Royal Meteorological Society 140 (684), 2197–2210.

[77] Uehara, K., Murakami, S., Oikawa, S., Wakamatsu, S., 2000. Wind tunnel experiments on how thermal stratification affects flow in and above urban street canyons. Atmospheric Environment 34 (10), 1553–1562.

[78] WHO, 2018. Ambient (outdoor) air quality and health. `https://www.who.int/news-room/factsheets/detail/ambient-(outdoor)-air-qualityand-health`, accessed: 2019-12-05.

[79] Xie, X., Liu, C.-H., Leung, D. Y., 2007. Impact of building façades and ground heating on wind flow and pollutant transport in street canyons. Atmospheric Environment 41 (39), 9030–9049.

[80] Yamartino, R. J., Wiegand, G., 1986. Development and evaluation of simple models for the flow, turbulence and pollutant concentration fields within an urban street canyon. Atmospheric Environment (1967) 20 (11), 2137–2156.